ACS Sustainable Chemistry & Engineering

Research Article

Cite This: ACS Sustainable Chem. Eng. 2018, 6, 12153−12165

pubs.acs.org/journal/ascecg

On the Validation of a One-Dimensional Biomass Pyrolysis Model Using Uncertainty Quantification

Himanshu Goyal*,† and Perrine Pepiot‡

†Robert F. Smith School of Chemical and Biomolecular Engineering, Cornell University, Ithaca, New York 14853, United States

‡Sibley School of Mechanical and Aerospace Engineering, Cornell University, Ithaca, New York 14853, United States

Supporting Information

ABSTRACT: Predictive modeling tools have the potential to accelerate the development and deployment of biomass thermochemical conversion. Considerable progress has been made in the modeling of biomass pyrolysis at the particle level, where chemical kinetics and transport processes are coupled. However, rigorous validation of the corresponding models is challenging because of the considerable uncertainty in the values of several biomass properties. Toward this end, we use the principles of uncertainty quantification (UQ) for a rigorous analysis of the validity of a commonly used one-dimensional wood pyrolysis model. Uncertainty in the modeling parameters of the transport processes is propagated to the simulation results of the pyrolysis model. The model predictions are compared with several detailed experimental measurements for pyrolysis of wood particles. The results show that the uncertainty in the model predictions account for some of the discrepancies with the experimental measurements, especially for the particle temperature profiles and the gas phase species production rates. Experimental targets are identified whose predictions cannot be improved by an accurate knowledge of the transport model parameters and require further improvements in the chemical kinetics model. The use of a systematic optimization technique is also demonstrated to choose the optimal values of uncertain model parameters.

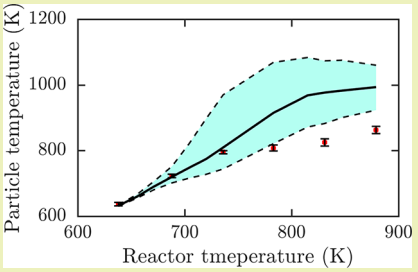

KEYWORDS: *Biomass pyrolysis, Model validation, Uncertainty quantification, Solution mapping, Optimization*

INTRODUCTION

Modeling and simulation tools provide a flexible and affordable framework to investigate the controlling chemical and physical processes of biomass pyrolysis, with the potential to play a determining role in the development and deployment of this conversion technique. Although modeling of biomass pyrolysis has come a long way, starting from one-component kinetic models[1] to a recently developed mechanistic model for cellulose pyrolysis,[2,3] a comprehensive understanding of biomass pyrolysis is far from reality, and a strong need for modeling efforts has been recognized in the literature.[4] Several challenges hinder the development of accurate models for biomass pyrolysis, a major one being the poor knowledge of the complex microscale morphological changes, such as shrinkage and changing internal particle structure, that take place inside a biomass particle during the pyrolysis process.[5] These morphological changes significantly affect biomass properties, such as thermal conductivity and heat capacity, and thus the transport of heat and mass.[6,7] Therefore, detailed particle level modeling of biomass pyrolysis requires models that can accurately capture the dependence of the biomass properties on the internal morphological changes.[8] However, such models do not yet exist because of the inherent complexity of the problem.[9]

Particle-scale models of biomass pyrolysis mathematically represent the chemical kinetics of the conversion process coupled with several intraparticle transport processes, such as the transport of mass and energy. The transport submodel requires biomass properties, such as thermal conductivity and specific heat capacity, as the input parameters. However, the variability in biomass feedstock and the scarcity of detailed data for biomass properties has prompted the usage of widely varying values for these properties in the literature.[10] Many times the biomass properties are tuned in an *ad-hoc* manner while validating the pyrolysis model.[11] A few studies, in the literature, have focused on relating the macroscopic properties of biomass to its microscopic structure. For instance, Eitelberger and Hofstetter[12] estimate the thermal conductivity of biomass close to room temperature using the biomass morphology and the thermal conductivities of its major constituents. However, the input parameters in their study are uncertain parameters and the effect of any morphological change is not included, which becomes important during biomass pyrolysis. For these reasons, the validation of biomass pyrolysis models has been identified as one of the "top ten" fundamental challenges of biomass pyrolysis by Mettler et al.[8] Considering the large uncertainties in the values of several biomass properties and their influence on biomass pyrolysis, uncertainty quantification (UQ) becomes an integral part of the model validation process. When the uncertainty in the model predictions is known, a meaningful comparison can be made with the experimental measurements, revealing specific parts of the model where further improvements should be sought.

Received: May 29, 2018
Revised: July 14, 2018
Published: July 14, 2018

DOI: 10.1021/acssuschemeng.8b02493
ACS Sustainable Chem. Eng. 2018, 6, 12153−12165

Many sources of uncertainty can exist in a model, such as boundary conditions, modeling assumptions, or model parameters.[13] The quantification of every single source of uncertainty present in a model is impractical, and generally, uncertainty in a few model parameters only is quantified and propagated to the model predictions.[14−16] In the case of biomass pyrolysis, although a detailed three-dimensional model has recently been developed,[17] a one-dimensional (1D) transport model coupled with a lumped chemical kinetic scheme is most commonly used to simulate particle-scale biomass pyrolysis experiments,[11,18−20] and different sources of uncertainty can be present in these 1D particle-scale models. In this study, we focus only on the uncertainty in the transport model parameters of woody biomass and neglect the other sources of uncertainty. The goal of this work is to provide an in-depth analysis of the validity of a 1D pyrolysis model against experiments considering the uncertainty in the transport model parameters and to find the optimal values of these uncertain parameters using a systematic optimization technique. To achieve this goal, we develop a 1D particle-scale pyrolysis model, quantify the uncertainty in the transport model parameters and propagate it to the model predictions.

Several UQ studies exist in the literature for different types of problems, such as combustion,[14] fluidized bed,[15] and coke gasifier,[16] yet, in our knowledge, no UQ study has been performed for biomass pyrolysis. For a detailed overview of various UQ methods, readers are referred to the review articles by Najm[13] and Wang and Sheen.[21] In this work, a nonintrusive UQ approach[14−16] is employed, where ensemble evaluations of the model are performed to propagate the uncertainty through the model. This brute force approach requires thousands of simulations to get the statistics of the output and would become computationally intractable if the original model is used for this purpose. To address this issue, the solution mapping (SM) method of Frenklach[22] is used to construct a response surface to estimate the predictions of the pyrolysis model in a computationally inexpensive manner. The SM method[22] is also used in the systematic optimization of the uncertain model parameters. It is important to note that while we focus here on transport parameters only, the methodology employed in this work can be applied in the same way to other modeling aspects related to industrially relevant biomass feedstock, such as shape and size of biomass particles.

The remainder of this paper is organized as follows. The Particle Model Description section describes the governing equations and boundary conditions of the one-dimensional particle-scale model for biomass pyrolysis used in this work. An overview of the methodology employed here to perform the UQ and optimization studies is provided in the Methodology section. The Results and Discussion section first presents two verification cases for the pyrolysis model, and then describes the results of the UQ and optimization studies. A detailed analysis of the results and their possible implications are also provided in this section.

PARTICLE MODEL DESCRIPTION

A spherically symmetric 1D intraparticle model, referred to as $\mathcal{M}_{\mathcal{P}}$, is developed for the simulation of wood pyrolysis based on the work of Park et al.[18] Here, both solid and gas phases are treated as a mixture of interpenetrating continua within the particle. During pyrolysis, the particle is heated through convection and/or radiation, releasing several gaseous species and gets converted into residual char. $\mathcal{M}_{\mathcal{P}}$ describes the conservation of mass in the gas and solid phases, the total energy of gas and solid phases, and individual gaseous species accompanying the pyrolysis of the particle. The lumped chemical kinetic scheme of the CRECK modeling group[11] is used to model the pyrolysis reactions. This kinetic scheme involves $n_s = 12$ solid species, 7 trapped gas species slowly releasing from the solid matrix, and $n_g = 20$ gaseous products. The initial composition of wood is represented by a combination of cellulose, hemicellulose, and three types of lignin. A brief description of the governing equations and the boundary conditions of $\mathcal{M}_{\mathcal{P}}$ are provided below.

The rate of change of mass per unit volume of the i^{th} solid component of the particle is given by

$$\frac{\mathrm{d}\rho_{s,i}}{\mathrm{d}t} = \omega_{s,i} \tag{1}$$

where $\rho_{s,i}$ is the apparent density (including pore volume) and $\omega_{s,i}$ is the reaction source term for the i^{th} solid component. Here, the particle shrinkage is assumed to be negligible,[23] making the particle radius constant and equal to the initial radius r_0. Mass conservation for the gas phase is given by

$$\frac{\partial(\varepsilon\rho)}{\partial t} + \frac{1}{r^2}\frac{\partial(r^2\rho U)}{\partial r} = \sum_{j=1}^{n_g}\omega_j \tag{2}$$

where ρ is the gas density, U is the superficial gas velocity, and ω_j is the source term for the j^{th} gas phase species. ε is the porosity, calculated by

$$\varepsilon = 1 - \frac{\rho_s}{\rho_s^0}(1 - \varepsilon_0) \tag{3}$$

In the equation above, ρ_s and ρ_s^0 are the instantaneous and initial solid masses per unit volume, respectively, and ε_0 is the initial particle porosity. A low Mach number assumption is made to remove the effect of pressure variations due to the gas flow on ρ. Assuming that the ideal gas law applies, ρ is calculated as

$$\rho = \frac{PM}{RT} \tag{4}$$

Here, P is the thermodynamic pressure, M is the molar mass of the gas phase mixture, and R is the ideal gas constant. Mass conservation for the j^{th} gas phase species is given by

$$\frac{\partial(\varepsilon\rho y_j)}{\partial t} + \frac{1}{r^2}\frac{\partial(r^2 U\rho y_j)}{\partial r} = \frac{1}{r^2}\frac{\partial}{\partial r}\left(r^2 D\frac{\partial\rho y_j}{\partial r}\right) + \omega_j \tag{5}$$

where y_j is the mass fraction of the j^{th} gas species, and D is the mass diffusivity, assumed to be constant for all species. Assuming a local thermodynamic equilibrium between gas and solid phases, the energy conservation equation can be written as

$$\left(\sum_{i=1}^{n_s}\rho_{s,i}C_i + \varepsilon\sum_{j=1}^{n_g}\rho_j C_{p,j}\right)\frac{\partial T}{\partial t} + \left(\sum_{j=1}^{n_g}\rho_j C_{p,j}\right)U\frac{\partial T}{\partial r} = \frac{1}{r^2}\frac{\partial}{\partial r}\left(r^2\lambda\frac{\partial T}{\partial r}\right) + \sum_{k=1}^{n_r}\Omega_k\Delta h_k \tag{6}$$

where T is the particle temperature, C_i is the specific heat capacity of the i^{th} solid component, and $C_{p,j}$ is the constant pressure specific heat capacity of the j^{th} gas phase species. Specific heat capacity of the gas phase $C_{p,g}$ is calculated as

DOI: 10.1021/acssuschemeng.8b02493
ACS Sustainable Chem. Eng. 2018, 6, 12153−12165

$\sum_{j=1}^{n_g} y_j C_{p,j}$. The last term on the right-hand side is the heat source term, where n_r is the total number of reactions, and Ω_k and Δh_k are the reaction rate and heat of reaction, respectively, of the k^{th} reaction. C for char is C_c and C for the rest of the solid components is assumed to be equal to the specific heat capacity of wood, C_w. Thermal conductivity for char is λ_c, and for the rest of the solid components, is assumed to be equal to the thermal conductivity of wood, λ_w. Both λ_w and λ_c are taken as the average value of the three directions (radial, tangential, and grain) of the particle. λ is the effective thermal conductivity, calculated as the weighted sum of the thermal conductivities of wood λ_w, char λ_c, and gases λ_g, and the radiative heat transfer through pores λ_{rad}.[18,24]

$$\lambda = (1-\gamma)\lambda_w + \gamma\lambda_c + \varepsilon\lambda_g + \lambda_{\text{rad}} \tag{7}$$

where λ_g is the mixture-averaged thermal conductivity of the gas phase, calculated as[25]

$$\lambda_g = \frac{1}{2}\left(\sum_{j=1}^{n_g} X_j\lambda_{g,j} + \frac{1}{\sum_{j=1}^{n_g} X_j/\lambda_{g,j}}\right) \tag{8}$$

Here, $\lambda_{g,j}$ and X_j are the thermal conductivity and the mole fraction of the j^{th} gaseous species, respectively. λ_{rad} is the contribution to the particle thermal conductivity due to the intraparticle radiation and is modeled following Di Blasi[24] as

$$\lambda_{\text{rad}} = \frac{13.5\sigma T^3 d}{e} \tag{9}$$

where σ is the Stefan−Boltzmann constant, e is the emissivity, and d is the effective pore size, calculated as

$$d = (1-\gamma)d_w + \gamma d_c \tag{10}$$

with d_w and d_c being the pore sizes of wood and char, respectively. γ is the degree of pyrolysis defined as

$$\gamma = 1 - \frac{\sum_{i=1}^{n_s}\rho_{s,i} - \rho_c}{\rho_s^0} \tag{11}$$

where ρ_c is the density of char.

At the particle boundary surface ($r = r_0$), species gradients are imposed by the external convective mass transfer, and the temperature gradient is imposed by the external convective and radiative heat transfer, such that

$$D\frac{\partial \rho y_j}{\partial r}\bigg|_{r=r_0} = \kappa(\rho y_{j,\infty} - \rho y_{j,r=r_0}) \tag{12}$$

$$\lambda\frac{\partial T}{\partial r}\bigg|_{r=r_0} = h(T_\infty - T_{r=r_0}) + \sigma e_s(T_{\text{reac}}^4 - T_{r=r_0}^4) \tag{13}$$

where e_s is the surface emissivity, and κ and h are the convective mass and heat transfer coefficients, respectively. $y_{j,r=r_0}$ is the mass fraction of the j^{th} gas phase species at the particle surface, $y_{j,\infty}$ is the ambient mass fraction of the j^{th} gas species, $T_{r=r_0}$ is the particle surface temperature, T_∞ is the ambient gas temperature, and T_{reac} is the wall temperature of the reactor where particle is heated. At the particle center ($r = 0$), a zero-gradient condition is imposed due to symmetry:

$$\frac{\partial T}{\partial r}\bigg|_{r=0} = 0 \tag{14}$$

$$\frac{\partial \rho y_j}{\partial r}\bigg|_{r=0} = 0 \tag{15}$$

The resulting set of coupled nonlinear partial differential equations (PDEs) is discretized using finite differences: a central difference scheme is used for the diffusion terms, while an upwind scheme is used for the convective terms. A backward Euler implicit scheme is employed to discretize the temporal terms. At each time step, all the discretized equations are solved iteratively until a converged solution is obtained. The verification of $\mathcal{M}_{\mathcal{P}}$ is provided in the Results and Discussion section.

METHODOLOGY

This section describes the methodology utilized to achieve our objectives of propagating the uncertainty in the transport model parameters to the predictions of $\mathcal{M}_{\mathcal{P}}$ and finding the optimal values of the uncertain model parameters.

The first step is to select a set of model parameters that is going to be used in the UQ study. To reduce the computational cost of performing the uncertainty analysis, only the transport model parameters contributing most to the uncertainty are included. To this end, a sensitivity analysis is performed to identify the most sensitive parameters, and the uncertainty in those sensitive parameters is quantified in the form of probability distribution functions (PDFs) using their values employed in the literature.

Since evaluating $\mathcal{M}_{\mathcal{P}}$ for multiple combinations of the uncertain model parameters is computationally expensive, the solution mapping (SM) method[22] is used to map the solution of $\mathcal{M}_{\mathcal{P}}$ to a multidimensional polynomial, known as response surface, allowing for a significant reduction in the cost of obtaining the output of $\mathcal{M}_{\mathcal{P}}$. In the SM method, each model parameter is normalized as

$$x_i = \frac{\ln(\mathcal{P}_i/\mathcal{P}_{i,0})}{\ln f_i} \tag{16}$$

where $\mathcal{P}_i$ is the i^{th} uncertain model parameter and $\mathcal{P}_{i,0}$, its nominal value. The normalization bounds x_i between −1 and +1 with its nominal value equal to 0. f_i is the uncertainty factor associated with $\mathcal{P}_i$, such that

$$\mathcal{P}_{i,0}/f_i \le \mathcal{P}_i \le \mathcal{P}_{i,0}f_i \tag{17}$$

For combustion problems, a second-order polynomial is usually adequate to be a response surface.[26] Considering the similarity between combustion and biomass pyrolysis in terms of the underlying physical and chemical processes, a second order polynomial is used here as well, and the response surface $\eta(\mathbf{x})$ is assumed to be of the form:

$$\eta(\mathbf{x}) = \eta_0 + \sum_{i=1}^{N} a_i x_i + \sum_{i=1}^{N}\sum_{j\ge i}^{N} b_{ij}x_i x_j \tag{18}$$

where N is the number of uncertain model parameters, and η_0 is the model prediction at the nominal values of the uncertain model parameters. a_i and b_{ij} are the constant polynomial coefficients, and are determined by conducting regression analysis of the output of several simulations of $\mathcal{M}_{\mathcal{P}}$, in which the values of uncertain model parameters are determined using a factorial design.[27] It should be noted that a separate $\eta(\mathbf{x})$

DOI: 10.1021/acssuschemeng.8b02493
ACS Sustainable Chem. Eng. 2018, 6, 12153−12165

needs to be created for each quantity of interest, such as particle temperature and species mass fraction, referred to as targets in this study.

To propagate the uncertainty in the model parameters to the predictions of $\mathcal{M}_{\mathcal{P}}$, evaluations of the response surface $\eta(\mathbf{x})$ are performed by sampling the PDFs of the normalized model parameters. Using the outputs of the response surface, a PDF is constructed for the predictions of a target.

The optimal values of the uncertain model parameters, which will be denoted by $\mathbf{x}^*$, are obtained by minimizing the least-squares difference between the experimental measurements η_i^{obs} and the model predictions $\eta_i(\mathbf{x})$ of the n targets of interest. This is done by minimizing the following objective function:

$$\mathbf{\Phi}(\mathbf{x}^*) = \min_{\mathbf{x}} \sum_{i=1}^{n} \left(\frac{\eta_i(\mathbf{x}) - \eta_i^{\text{obs}}}{\eta_i^{\text{obs}}} \right)^2 \tag{19}$$

subject to the constraint that $-1 \leq x_i \leq +1$. In general, the standard deviation σ_i^{obs} in the experimental measurements is preferred to normalize the differences between the measurements and the predictions, as it includes the inherent uncertainty in the experimental measurements and hence, can provide better weighting factors for different targets. In this study, σ_i^{obs} for all the experimental data used is not available, therefore, in eq 19, the differences between the measurements and the predictions are normalized by η_i^{obs}.

RESULTS AND DISCUSSION

The methodology described in the previous section is now employed to quantify the uncertainties in the prediction of model $\mathcal{M}_{\mathcal{P}}$ and provide a more comprehensive and insightful comparison of those predictions with experimental data. As mentioned above, we focus here on the influence of the uncertainty in the values of the transport model parameters only.

The results are presented in three subsections. The first subsection provides two verification cases for $\mathcal{M}_{\mathcal{P}}$ by comparing its predictions with the analytical solution of the 1D transient heat conduction in a sphere and the results of a similar 1D model implemented in COMSOL Multiphysics[28] by Corbetta et al.[11] In the second subsection, the results of the UQ study are provided and analyzed in the context of a comparison with experimental data. In the third subsection, optimal values for the uncertain model parameters are evaluated and the predictions of the resulting optimized model $\mathcal{M}_{\mathcal{P}}^*$ and unoptimized/base model $\mathcal{M}_{\mathcal{P}}$ are compared.

In this work, two experimental studies are used for the UQ and optimization studies: (1) the pyrolysis of maple wood spheres with diameter d_p = 2.54 cm by Park et al.[18] at six reactor temperatures T_{reac}: 638, 688, 736, 783, 831, and 879 K, which will be referred to as experimental set $\mathcal{E}_{\text{I}}$, and 2) the pyrolysis of poplar wood spheres with d_p = 2.54 cm by Bennadji et al.[29] at T_{reac} = 641, 700, and 743 K, referred to as experimental set $\mathcal{E}_{\text{II}}$. As both the experimental studies were performed at low reactor temperatures, secondary gas phase reactions are assumed to be negligible and not considered in the simulations. In $\mathcal{E}_{\text{I}}$, measurements include the evolution of temperature at different locations inside the particle and solid mass fraction, and the final lumped product yields. In $\mathcal{E}_{\text{II}}$, the instantaneous production rates and the yields of CO, CO_2, CH_4, HCHO, HCOOH, and CH_3COOH are measured. Table 1 provides the targets selected from $\mathcal{E}_{\text{I}}$ and $\mathcal{E}_{\text{II}}$ for both the UQ and the optimization studies. In this table, t_{dev} is defined as the time at which the rate of change of solid mass fraction becomes very small (a cutoff value of 10^{-4} is used in the simulations). The lumped product yield of gas, $Y_{\text{gas}}^{\text{lump}}$, is defined as the sum of the yields of all the permanent gaseous species, such as CO and CH_4, included in $\mathcal{M}_{\mathcal{P}}$, whereas the lumped product yield of tar, $Y_{\text{tar}}^{\text{lump}}$, is taken as the sum of the yields of all the species that are liquid at room temperature, such as levoglucosan.

Table 1. Selected Targets from $\mathcal{E}_{\text{I}}$ and $\mathcal{E}_{\text{II}}$ for the UQ and Optimization Studies

Targets for $\mathcal{E}_{\text{I}}$	Targets for $\mathcal{E}_{\text{II}}$
(1) Peak temperature at the particle center, T_{peak}	(1) Peak production rate of species, $\mathcal{P}$
(2) Time of peak temperature at the particle center, $t_{T_{\text{peak}}}$	(2) Time of peak production rate of species, $t_{\mathcal{P}}$
(3) Devolatilization time, t_{dev}	(3) Yield of species, $\mathbf{Y}$
(4) Lumped product yields, $\mathbf{Y}^{\text{lump}}$: $Y_{\text{gas}}^{\text{lump}}$, $Y_{\text{tar}}^{\text{lump}}$, and solid residue (SR)	

Verification of the Particle Model. For the first verification case, the predictions of $\mathcal{M}_{\mathcal{P}}$ are compared with the analytical solution of the 1D transient heat conduction in a sphere with constant properties. For the comparison, a spherical particle with r_0 = 5 mm, density ρ_p = 630 kg/m^3, specific heat capacity C = 1800 J/(kg·K), initial particle temperature T_0 = 300 K, and ambient temperature T_∞ = 773 K is considered. The analytical solution for the temperature evolution inside the sphere is given by[30]

$$\theta = \sum_{i=1}^{\infty} C_i \exp(-\zeta_i^2 Fo) \frac{\sin(\zeta_i r^*)}{\zeta_i r^*}$$

$$C_i = \frac{4[\sin(\zeta_i) - \zeta_i \cos(\zeta_i)]}{2\zeta_i - \sin(2\zeta_i)},\ 1 - \zeta_i \cot(\zeta_i) = Bi \tag{20}$$

Here, $\theta = \frac{T - T_\infty}{T_0 - T_\infty}$ is the nondimensional temperature, and r^* is the radial location normalized by r_0: $r^* = r/r^0$. Bi is the Biot number, defined as $Bi = hr_0/\lambda$, Fo is the Fourier number, equivalent to a dimensionless time and defined as $\alpha\, t/l^2$, where t is the time, α is the thermal diffusivity, and l is the characteristic length defined as $r_0/2$. For $Fo > 0.2$, the series solution in eq 20 can be approximated by its first term:[30]

$$\theta = C_1 \exp(-\zeta_1^2 Fo) \frac{\sin(\zeta_1 r^*)}{\zeta_1 r^*} \tag{21}$$

Using the values of ζ_1 and C_1 taken from Bergman et al.,[30] the analytical solution for the temperature evolution at the particle center is fully determined. Figure 1 shows the comparison of the analytical solution with the predictions of $\mathcal{M}_{\mathcal{P}}$ for a wide range of Bi. As expected, the numerical solution of $\mathcal{M}_{\mathcal{P}}$ is in excellent agreement with the analytical solution.

In the second verification case, we compare the predictions of $\mathcal{M}_{\mathcal{P}}$ with those of a similar 1D particle model implemented in COMSOL Multiphysics[28] by Corbetta et al.[11] to simulate the pyrolysis of the maple wood spheres used in the $\mathcal{E}_{\text{I}}$ experimental set. We use $\mathcal{M}_{\mathcal{P}}$ to simulate the same experiments with the values of model parameters taken from Corbetta et al.[11] and provided in the Supporting Information document. Figure 2 shows the comparison between the predictions of $\mathcal{M}_{\mathcal{P}}$ and

DOI: 10.1021/acssuschemeng.8b02493
ACS Sustainable Chem. Eng. 2018, 6, 12153−12165

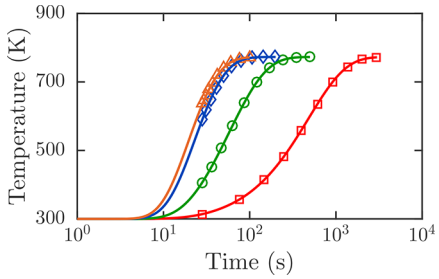

Figure 1. Temperature evolution for 1D transient heat conduction in a solid sphere. Comparison between the predictions of $\mathcal{M}_{\mathcal{P}}$ (lines) and the analytical expression (symbols) for the center temperature. Different symbols indicate different *Bi* (red square, 10^{-1}; green circle, 10^{0}; blue diamond, 10^{1}; orange triangle, 10^{2}).

those of the COMSOL simulation of Corbetta et al.,[11] along with the measurements from $\mathcal{E}_{\mathrm{I}}$. The excellent agreement between the predictions of $\mathcal{M}_{\mathcal{P}}$ and the COMSOL simulations[11] further verifies the numerical implementation of $\mathcal{M}_{\mathcal{P}}$.

Uncertainty Quantification. *Uncertain Model Parameters.* Performing the uncertainty analysis for a large number of model parameters is computationally intractable. For this reason, we only consider those transport model parameters that (1) show large sensitivity to the model predictions, and (2) have large uncertainty in their values. To identify the most sensitive model parameters, a sensitivity analysis of $\mathcal{M}_{\mathcal{P}}$ is performed for the experimental conditions of $\mathcal{E}_{\mathrm{I}}$ at the lowest (T_{reac} = 638 K) and the highest (T_{reac} = 831 K) reactor temperatures. The sensitivity coefficient associated with the i^{th} model parameter $\mathcal{P}_i$, $\mathcal{S}_{i,j}$, is defined as

$$\mathcal{S}_{i,j} = \frac{\mathcal{P}_{i,0}}{\mathcal{P}_i - \mathcal{P}_{i,0}} \frac{\mathcal{G}_j - \mathcal{G}_{j,0}}{\mathcal{G}_{j,0}} \tag{22}$$

where $\mathcal{P}_{i,0}$ is the nominal value of the model parameter and $\mathcal{P}_i$ is obtained by multiplying $\mathcal{P}_{i,0}$ with a factor χ. $\mathcal{G}_j$ and $\mathcal{G}_{j,0}$ are the model predictions of the j^{th} target corresponding to $\mathcal{P}_i$ and $\mathcal{P}_{i,0}$, respectively. We choose χ = 2 to calculate $\mathcal{S}_{i,j}$. Figure 3 plots the coefficients $\mathcal{S}_{i,j}$ for the targets: T_{peak}, t_{dev}, and $\mathbf{Y}^{\mathrm{lump}}$. We observe that at T_{reac} = 879 K, $\mathcal{M}_{\mathcal{P}}$ is sensitive to a larger number of model parameters and exhibits higher sensitivity compared to T_{reac} = 638 K. For the purpose of this study, the model parameters with $\mathcal{S}_{i,j} > 0.05$ at both temperatures for at least one target are selected. Six model parameters are found to satisfy this criterion: λ_w, λ_c, C_w, C_c, λ_g, and $C_{p,g}$. Out of these six sensitive parameters, λ_g and $C_{p,g}$ are known with relatively low uncertainty as the properties of the gas species involved in our case have typically been studied, extensively. The remaining four sensitive model parameters correspond to the thermal properties of biomass. Several sensitivity studies[31,32] in the literature have also identified the thermal properties to be the most sensitive parameters in a particle-level pyrolysis model, and these properties also show high variability in their reported values in the literature.[31−34] Therefore, we choose $\mathcal{H}$: {λ_w, λ_c, C_w, C_c} as the set of uncertain model parameters for the UQ study.

Uncertainty Characterization in Selected Model Parameters. In the literature, due to the lack of the detailed measurements of thermal conductivities and heat capacities for various biomass samples, modelers commonly use the values of these properties measured at low temperatures available for other biomass samples[35] or tune these properties to obtain a better match with the experiments.[11] Therefore, we used various expressions and values of λ_w, λ_c, C_w, and C_c reported in the literature (listed in Table 2) as a way to estimate the uncertainty in these properties. In Table 2, $\lambda_{w,\parallel}$ and $\lambda_{w,\perp}$ are the wood thermal conductivity parallel and perpendicular to the grain direction, respectively. In the literature, an average value of wood thermal conductivity λ_w is obtained by a linear combination of $\lambda_{w,\parallel}$ and $\lambda_{w,\perp}$ using some empirical weighting coefficients.[17] Because we want to estimate a broad range of values of λ_w used in the literature, $\lambda_{w,\parallel}$ and $\lambda_{w,\perp}$ are simply considered to be the possible values of λ_w. In general, C_w and C_c are expressed as functions of temperature, whereas constant

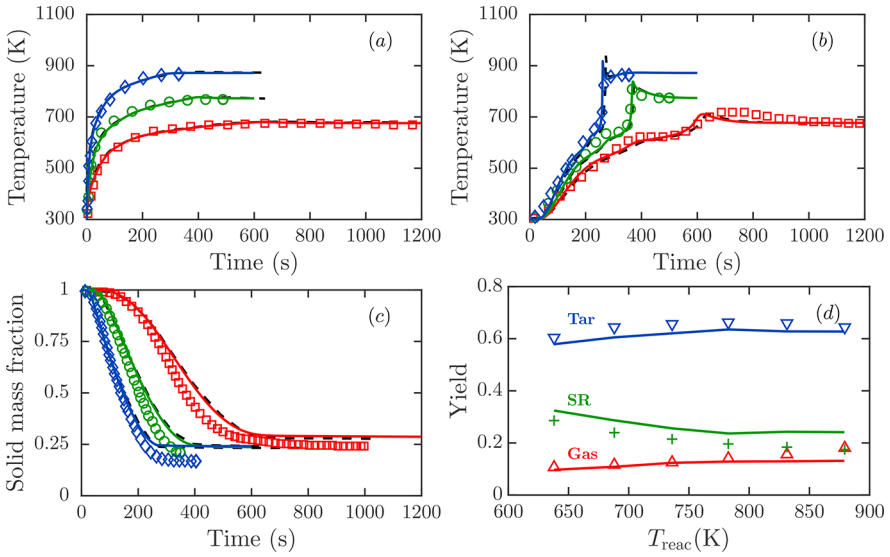

Figure 2. Comparison between the predictions of $\mathcal{M}_{\mathcal{P}}$ (solid lines) and COMSOL simulations results (Corbetta et al.,[11] dashed lines), along with the measurements from $\mathcal{E}_{\mathrm{I}}$ (symbols). Panels a, b, and c show the evolution as a function of time of the particle surface temperature, the particle center temperature, and solid mass fraction, respectively. Different symbols indicate different reactor temperatures T_{reac} (red square, 688 K; green circle, 783 K; blue diamond, 879 K). Panel d shows the lumped product yields as a function of T_{reac}.

DOI: 10.1021/acssuschemeng.8b02493
ACS Sustainable Chem. Eng. 2018, 6, 12153−12165

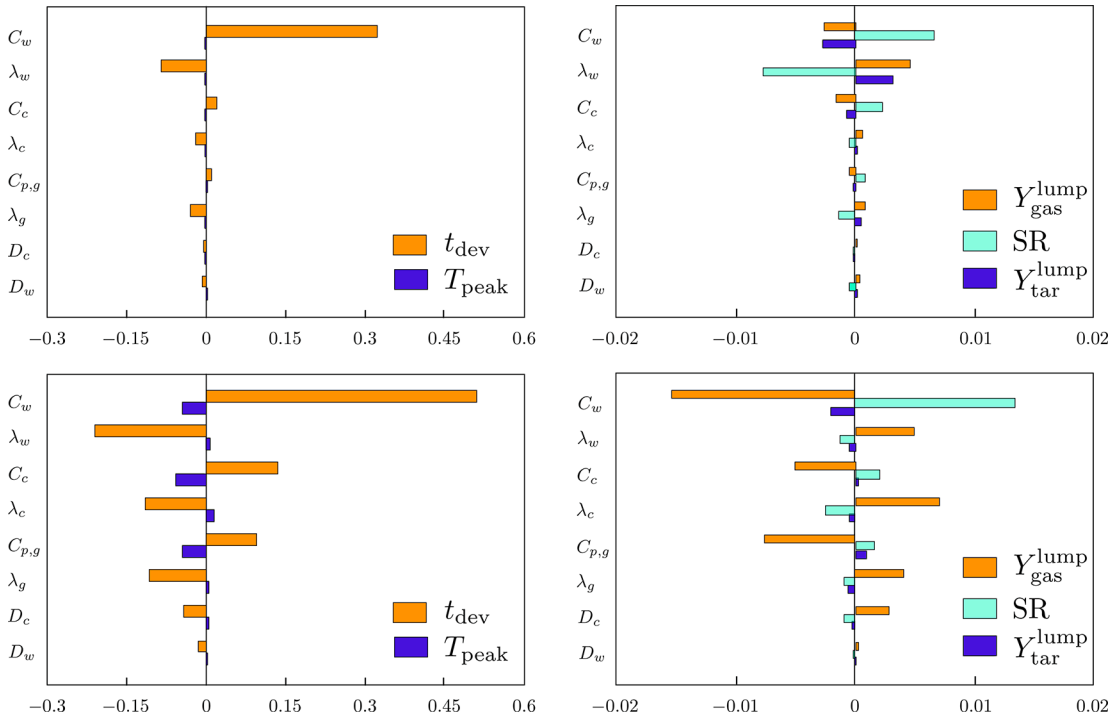

Figure 3. Sensitivity analysis of $\mathcal{M}_{\mathcal{P}}$ for $\mathcal{E}_{\mathrm{I}}$. Top row: T_{reac} = 638 K and Bottom row: T_{reac} = 879 K.

Table 2. Values and Expressions Used in the Literature for C_w, C_c, λ_w, and λ_c

Specific heat capacity of wood C_w (kJ/kg·K)	
2.3	ref. 38−41
$2.3-1.15\exp(-0.0055T)$	ref. 42
$-0.0912 + 0.0044T$	ref. 43
$1.2 + 2.45 \times 10^{-3}(T - 273)$	ref. 44
$0.2316 + 3.69 \times 10^{-3}T$	ref. 33
$1.5 + 10^{-3}T$	ref. 11, 17, 18, 45
$0.1031 + 3.867 \times 10^{-3}T$	ref. 46, 47
$0.112 + 4.85 \times 10^{-3}T$	ref. 48, 49
Specific heat capacity of char C_c (kJ/kg·K)	
1.1	ref. 38−41
$1.39 + 3.6 \times 10^{-4}T$	ref. 46, 50
$1.430 + 3.55 \times 10^{-4}T - 7.32 \times 10^{4}\ T^{-2}$	ref. 42, 51,52
$1.0032 + 2.09 \times 10^{-3}(T - 273)$	ref. 48, 49
$0.42 + 2.09 \times 10^{-3}T + 6.85 \times 10^{-3}T^2$	ref. 45
$-0.79528 + 5.98 \times 10^{-3}T - 3.8 \times 10^{-6}T^2$	ref. 33
Thermal conductivity of wood λ_w (W/m·K)	
0.1256	ref. 39, 53
0.11	ref. 35,54
$\lambda_{w,\parallel} = 0.73, \lambda_{w,\perp} = 0.52$	ref. 42, 55
$0.13 + 3 \times 10^{-4}(T - 273)$	ref. 48, 49
$\lambda_{w,\perp} = 0.0986$	ref. 33
$\lambda_{w,\parallel} = 0.156-0.278, \lambda_{w,rad} = 0.112-0.176, \lambda_{w,tan} = 0.074-0.133$	ref. 56
$\lambda_{w,\parallel} = 0.158-0.419, \lambda_{w,\perp} = 0.081-0.209$	ref. 45
$\lambda_{w,\parallel} = 0.291-0.323, \lambda_{w,\perp} = 0.177-0.214$	ref. 57
$\lambda_{w,\parallel} = 0.2-0.4, \lambda_{w,\perp} = 0.1-0.25$	ref. 55
Thermal conductivity of char λ_c (W/m·K)	
0.052	ref. 46
0.0837	ref. 39, 53
0.071	ref. 35, 54
0.1405	ref. 11
$0.08-10^{-4}(T - 273)$	ref. 48, 49

values are used for λ_w and λ_c, even though both λ_w and λ_c are known to increase with temperature.[33,36]

The uncertainty in the value of a model parameter is represented by a probability density function (PDF), with normal and uniform distributions being the two limiting cases.[37] If the values of a parameter are measured a statistically significant number of times such that a meaningful standard deviation can be defined, then the parameter values should be assumed to have a normal distribution. On the other hand, if only a few measurements are available to provide an estimate of lower and upper bounds, then the parameter should be assumed to have a uniform distribution.[37] In this work, the latter is true for the parameters in $\mathcal{H}$, and their values are therefore assumed to be uniformly distributed.

For uniformly distributed model parameter values, $\mathcal{P}_{i,0}$ and f_i can be estimated from eq 17 using their minima and maxima from Table 2:

$$f_i = \sqrt{\frac{\mathcal{P}_{i,\max}}{\mathcal{P}_{i,\min}}} \quad \text{and} \quad \mathcal{P}_{i,0} = \sqrt{\mathcal{P}_{i,\max}\mathcal{P}_{i,\min}} \tag{23}$$

eq 23 provides single values of f_i and $\mathcal{P}_{i,0}$ for λ_w and λ_c, whereas for C_w and C_c, f_i and $\mathcal{P}_{i,0}$ vary with temperature. We found that the nominal values of C_w and C_c can be closely predicted by the expressions of Gupta et al.[33] and Fredlund et al.,[51] respectively. We use the maxima of f_i for both C_w and C_c as their respective uncertainty factors. Figure 4 shows the values of C_w and C_c obtained from the various expressions provided in Table 2 along with the nominal values, $\mathcal{P}_{i,0}$, and the lower $(\mathcal{P}_{i,0}/f_i)$ and upper $(\mathcal{P}_{i,0}f_i)$ limits of their distributions. Table 3 provides $\mathcal{P}_{i,0}$ and f_i estimated for all the parameters in $\mathcal{H}$.

Response Surface. A response surface $\eta(\mathbf{x})$ is created for each experimental target of $\mathcal{E}_{\mathrm{I}}$ and $\mathcal{E}_{\mathrm{II}}$ using the full 2^N factorial design, requiring $2^N + 2N + 1$ simulations of $\mathcal{M}_{\mathcal{P}}$.[27] In this work, N = 4 (C_w, C_c, λ_w, and λ_c) and thus 25 computational

DOI: 10.1021/acssuschemeng.8b02493
ACS Sustainable Chem. Eng. 2018, 6, 12153−12165

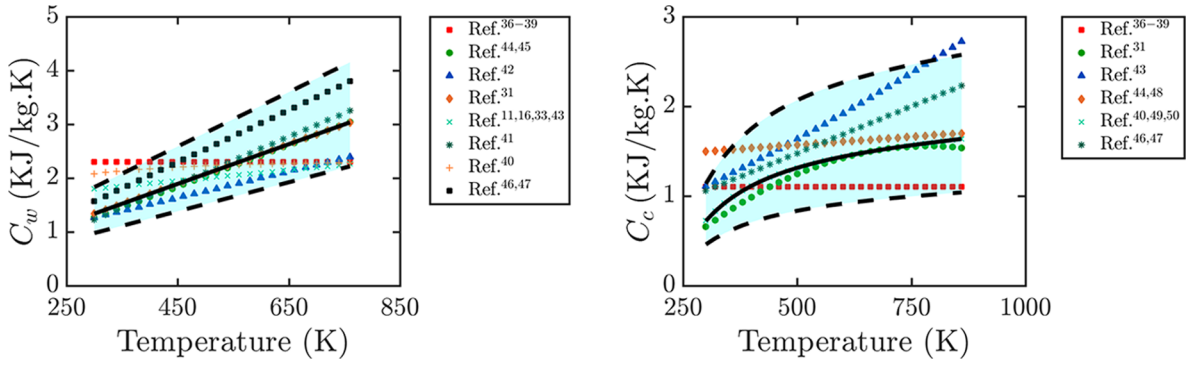

Figure 4. C_w and C_c from various sources. Different symbols correspond to expressions for C_w and C_c provided in Table 2. The nominal values $\mathcal{P}_{i,0}$ are shown by solid lines, while the minimum $\mathcal{P}_{i,\min}$ and maximum $\mathcal{P}_{i,\max}$ values are shown by dashed lines.

Table 3. Uncertain Model Parameters with Their Nominal Values and Uncertainty Factors

Parameter in $\mathcal{H}$	Units	Nominal value, $\mathcal{P}_{i,0}$	Uncertainty factor, f_i
λ_w	W/(m·K)	0.232	3.1
λ_c	W/(m·K)	0.085	1.6
C_w	J/(kg·K)	$231.6 + 3.69T$	1.8
C_c	J/(kg·K)	$1430 + 0.355T - 7.32 \times 10^7\ T^{-2}$	1.4

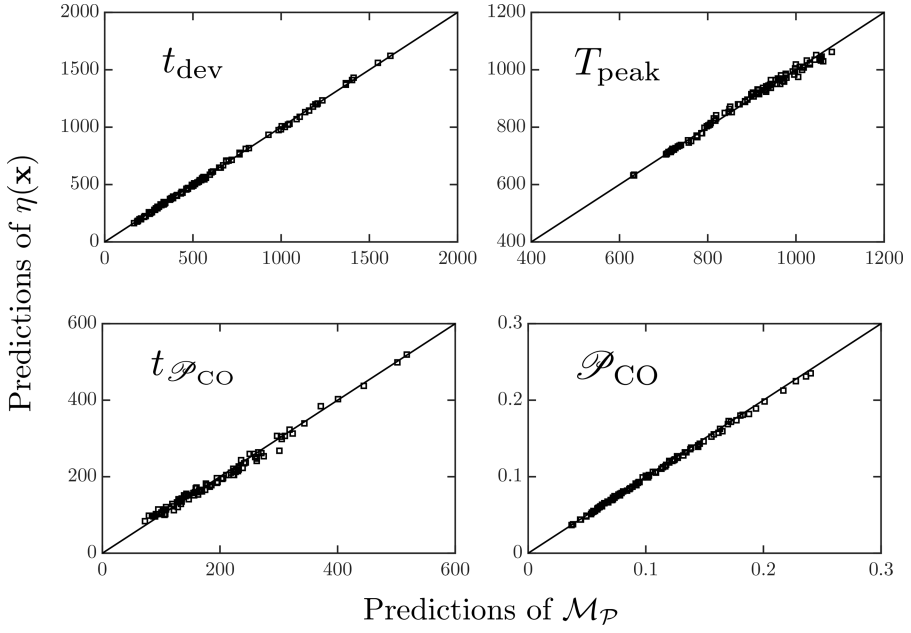

Figure 5. Comparison of response surface $\eta(\mathbf{x})$ predictions vs direct calculations using $\mathcal{M}_{\mathcal{P}}$.

runs of $\mathcal{M}_{\mathcal{P}}$ are required to create the response surfaces for all the targets of an experiment at a single reactor temperature. The simulation parameters are taken from Corbetta et al.[11] and are provided in the Supporting Information document. To check the adequacy of the created response surfaces, their predictions for each target are compared with those of $\mathcal{M}_{\mathcal{P}}$ by sampling from the PDFs of the parameters in $\mathcal{H}$. Correlation coefficients are calculated between the predictions of $\eta(\mathbf{x})$ and $\mathcal{M}_{\mathcal{P}}$, and are found to be greater than 0.99 for every target, confirming that the response surfaces provide adequate estimates for the predictions of $\mathcal{M}_{\mathcal{P}}$. Figure 5 shows the comparison between the predictions of $\eta(\mathbf{x})$ and $\mathcal{M}_{\mathcal{P}}$ for t_{dev}, T_{peak}, $t_{\mathcal{P}_{\text{CO}}}$, and $\mathcal{P}_{\text{CO}}$.

Uncertainty in the Model Predictions. Response surfaces $\eta(\mathbf{x})$ developed in the previous subsection are evaluated for $\mathbf{x}$ sampled from the PDFs of the parameters in $\mathcal{H}$ to propagate the input uncertainty through $\mathcal{M}_{\mathcal{P}}$. For this purpose, 100,000 samples are used for each target, and are found to be sufficient to get converged statistics. The resulting model outputs are used to construct the PDF and cumulative density function (CDF) of each target's predictions. To quantify the uncertainty in the model predictions, we calculate the mean, and the lower l_b and upper u_b bounds of the model predictions of a target containing 95% area of the PDF. Consequently, $F(l_b) = 0.025$ and $F(u_b) = 0.975$, where F is the CDF of the target's predictions. The predictions of $\mathcal{M}_{\mathcal{P}}$ including the uncertainty are compared with the experimental measurements for the targets of $\mathcal{E}_{\text{I}}$ and $\mathcal{E}_{\text{II}}$ as shown in Figures 6, 7, 8, and 9. Figure 6 shows the comparison for the targets of $\mathcal{E}_{\text{I}}$: $t_{T_{\text{peak}}}$, T_{peak}, t_{dev}, and $\mathbf{Y}^{\text{lump}}$, whereas Figures 8, 7, and 9 show the comparison for the

DOI: 10.1021/acssuschemeng.8b02493
ACS Sustainable Chem. Eng. 2018, 6, 12153−12165

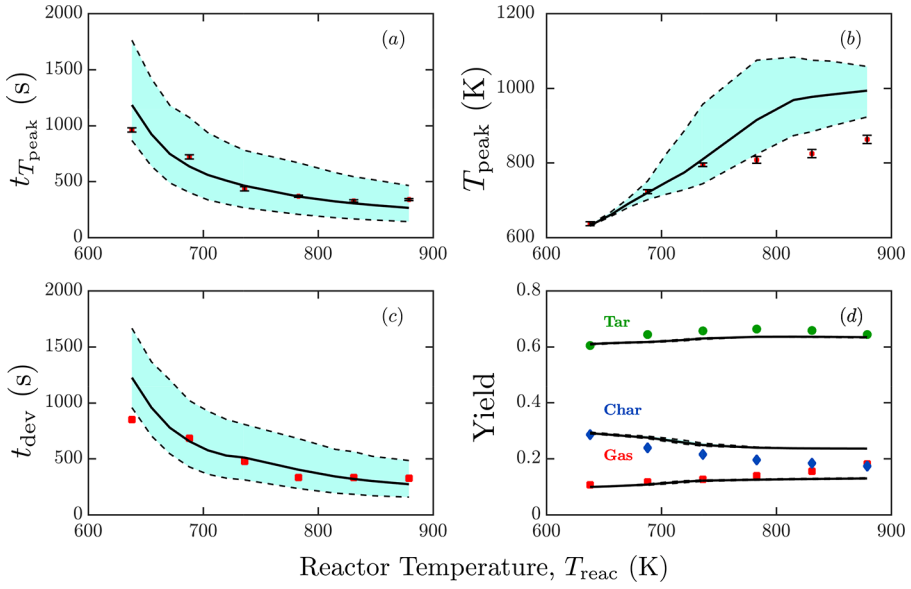

Figure 6. Comparison between the predictions of $\mathcal{M}_{\mathcal{P}}$ (solid lines: mean; dashed lines: 95% coverage of uncertainty) and the experimental measurements (symbols, $\mathcal{E}_{I}$).

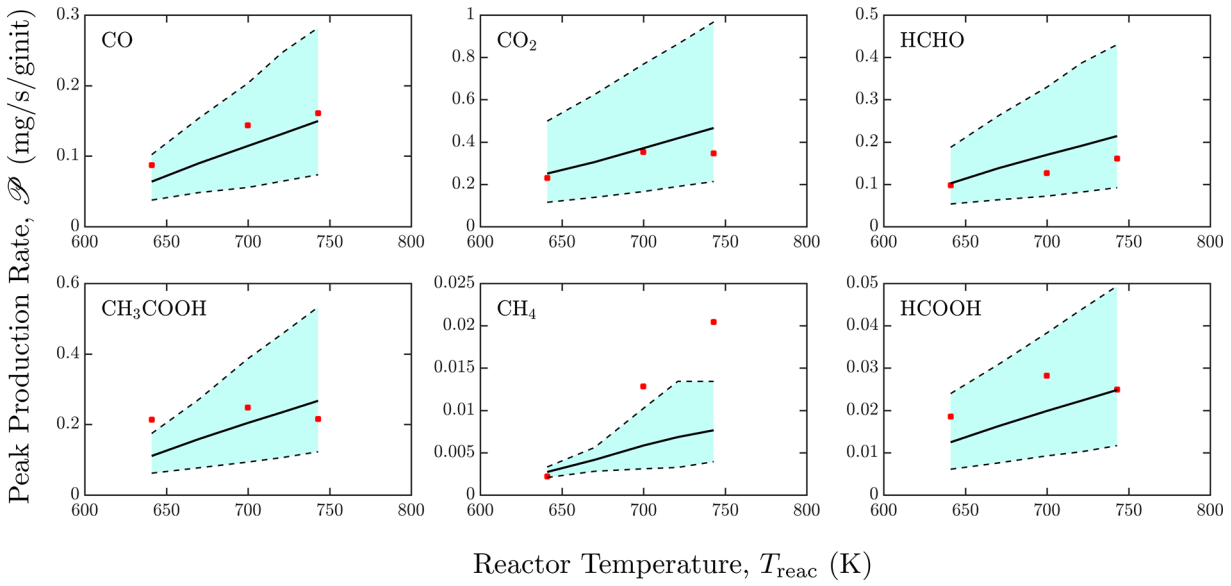

Figure 7. Comparison of the experimental measurements (symbols, $\mathcal{E}_{II}$) and the predictions of $\mathcal{M}_{\mathcal{P}}$ (solid lines: mean; dashed lines: 95% coverage of uncertainty) for peak production rates of different species, $\mathcal{P}$.

targets of $\mathcal{E}_{II}$: $\mathcal{P}$, $t_{\mathcal{P}}$, and $\mathbf{Y}$, respectively. The error bars for the experimental measurements are added to the figures whenever available.

Figures 6–9 show that significant uncertainty exists in the model predictions of all the targets except for $\mathbf{Y}^{lump}$ and $\mathbf{Y}$. This is expected, because the sensitivity analysis predicted small sensitivity of the product yields toward the transport model parameters (Figure 3). We also observe that the uncertainty bounds are proportional to the mean values for most of the targets; however, a nonlinear dependence is observed for T_{peak} and $t_{\mathcal{P}}$ as shown in Figure 6(b) and Figure 8, respectively. This observation emphasizes the fact that the model output can have a nonlinear dependence on the model parameters, which may not be captured by a simple sensitivity analysis.

Figure 6 shows that most of the discrepancy between the experimental measurements and the model predictions of $t_{T_{peak}}$ and t_{dev} can be attributed to the uncertainty in the model predictions, whereas the same is true for T_{peak} only when T_{reac} < 783 K. In the experiments $\mathcal{E}_{I}$, a steep temperature rise is observed at the particle center exceeding the surface temperature (Figure 2(b)), which has been linked to the exothermic decomposition of the intermediate solids formed during the pyrolysis process.[18] In $\mathcal{E}_{I}$, this overshoot of the center temperature above the surface temperature is found to first increase and then decrease with T_{reac}, becoming maximum at T_{reac} = 736 K, whereas $\mathcal{M}_{\mathcal{P}}$ predicts the temperature overshoot to continuously increase with T_{reac}. This observation may explain why $\mathcal{M}_{\mathcal{P}}$ fails to predict T_{peak} when $T_{reac} \geq$ 783 K. Improvements in the predictions of T_{peak} for $T_{reac} \geq$ 783 K can be a focus area for further developments in the chemical kinetic model, as the uncertainty in the transport model parameters

DOI: 10.1021/acssuschemeng.8b02493
ACS Sustainable Chem. Eng. 2018, 6, 12153−12165

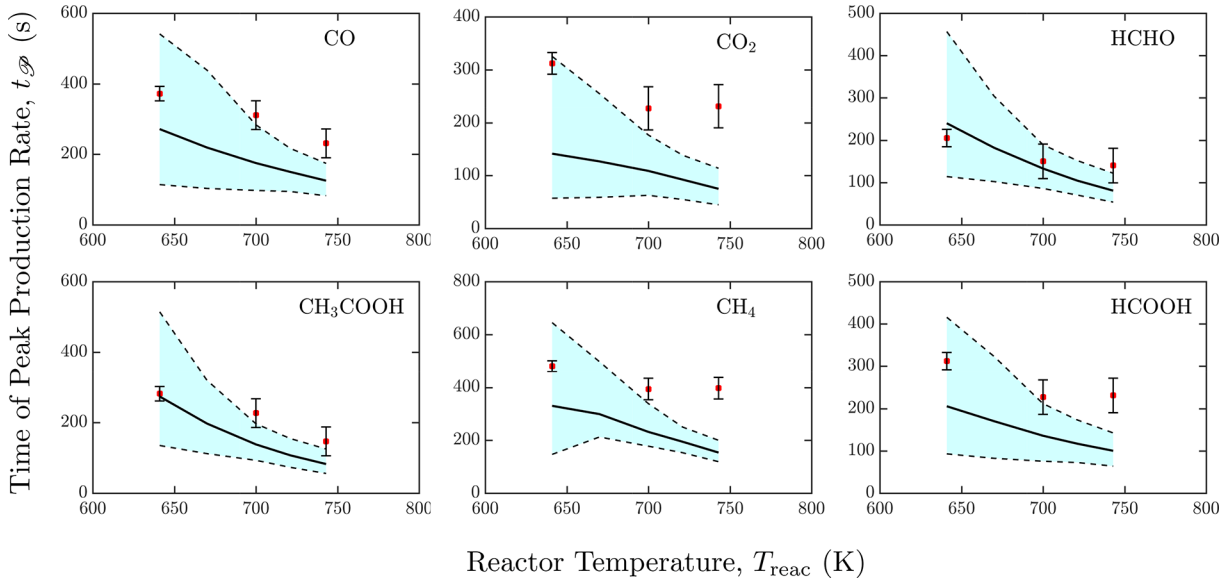

Figure 8. Comparison of the experimental measurements (symbols, $\mathcal{E}_{II}$) and the predictions of $\mathcal{M}_{\mathcal{P}}$ (solid lines, mean; dashed lines, 95% coverage of uncertainty) for time of peak production rate of different species, $t_{\mathcal{P}}$.

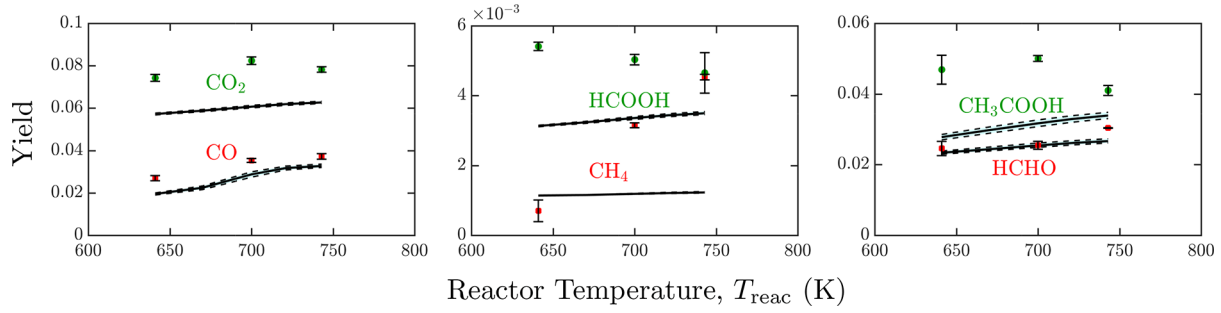

Figure 9. Comparison of the experimental measurements (symbols, $\mathcal{E}_{II}$) and the predictions of $\mathcal{M}_{\mathcal{P}}$ (solid lines: mean; dashed lines: 95% coverage of uncertainty) for yields of different species, $\mathbf{Y}$.

can not explain the discrepancy for it. Figure 6(d) shows that the negligible uncertainty in the predictions of $\mathbf{Y}^{lump}$ cannot explain the observation that $\mathcal{M}_{\mathcal{P}}$ overpredicts the yield of SR, yet underpredicts Y_{gas}^{lump}. The discrepancy in the product yields has been observed in the literature and to some extent, has been linked to an inadequate representation of the chemisorbed species.[58,59]

Figure 7 shows that $\mathcal{M}_{\mathcal{P}}$ can accurately predict $\mathcal{P}$ within the uncertainty bounds for all species except CH_4. However, significant discrepancy exists between the experiments and the model predictions of $t_{\mathcal{P}}$ for CO_2, CH_4, and HCOOH at $T_{reac} \geq$ 700 K as shown in Figure 8. Also, the mean values of the predictions of $t_{\mathcal{P}}$ are found to be smaller than most of the experimental measurements. The results for $\mathcal{P}$ and $t_{\mathcal{P}}$ imply that even though $\mathcal{M}_{\mathcal{P}}$ is able to predict the peak production rates of most species within the uncertainty bounds, it tends to underpredict the timings of species production, especially for CO_2, CH_4, and HCOOH. Similar to the case of $\mathbf{Y}^{lump}$, the uncertainty in the predictions of $\mathbf{Y}$ is negligible as shown in Figure 9. $\mathcal{M}_{\mathcal{P}}$ underpredicts the yields of all the gas species, and the deviations with the experimental measurements are up to a factor of 4 for CH_4, and within a factor of 2 for other species. The results presented in Figures 7−9 show that $\mathcal{M}_{\mathcal{P}}$ performs poorly for the predictions of all the targets related to CH_4. In the literature, other studies have also reported the inability of the chemical kinetic model used in this work to accurately predict the evolution of CH_4 and light hydrocarbons.[11,58,59] In the kinetic model, CH_4, as well as other light hydrocarbons, are mainly produced in the form of chemisorbed species releasing slowly from the solid matrix. The main reason for adding these chemisorbed species in the kinetic model was to match the mass loss data observed experimentally, and their kinetic parameters remain partially adaptive.[11] The uncertainty analysis shows that the kinetics of the chemisorbed species require further development to improve the predictions of CH_4 and probably other light hydrocarbons.

The uncertainty analysis for $\mathcal{E}_I$ shows that the model predictions related to the particle temperature profiles are, in general, in good agreement with the experiments if the uncertainty in the model predictions is included. However, a few targets such as T_{peak} for T_{reac} > 783 K and the yields of Gas and SR require further improvements in the pyrolysis model. The UQ results for $\mathcal{E}_{II}$ show that $\mathcal{M}_{\mathcal{P}}$ performs poorly for all the targets related to CH_4. Also, the predictions of the species yields and $t_{\mathcal{P}}$ for CO_2, CH_4, and HCOOH need to be improved. Moreover, for both $\mathcal{E}_I$ and $\mathcal{E}_{II}$, the predictive ability of $\mathcal{M}_{\mathcal{P}}$ is observed to decrease at higher temperatures. Further improvements in the chemical kinetic model focusing on the

DOI: 10.1021/acssuschemeng.8b02493
ACS Sustainable Chem. Eng. 2018, 6, 12153−12165

targets described here are likely needed to improve the predictive ability of the 1D pyrolysis model.

Optimization of the Uncertain Model Parameters. Uncertainty in the model parameters provides some flexibility in tuning them to improve the model predictions. In the biomass literature, the tuning of the model parameters is usually done in an *ad-hoc* manner. In this work, the optimal values of the parameters included in set $\mathcal{H}$ are estimated by minimizing the objective function $\Phi(\mathbf{x})$ defined in eq 19 using the default nonlinear optimization solver in GAMS,[60] a commercial software to solve optimization problems. The obtained optimal values of the parameters in $\mathcal{H}$ are provided in Table 4.Comparisons

Table 4. Optimal Values of the Uncertain Model Parameters

Model parameters in $\mathcal{H}$	Units	Optimal values of the parameters in $\mathcal{H}$
λ_w	W/(m·K)	0.471
λ_c	W/(m·K)	0.136
C_w	J/(kg·K)	$412.5 + 6.57T$
C_c	J/(kg·K)	$1218 + 0.301T - 6.20 \times 10^7\ T^{-2}$

of the predictions of the targets obtained from $\mathcal{M}_{\mathcal{P}}^{*}$ and $\mathcal{M}_{\mathcal{P}}$ are shown in Figure 10 for $\mathcal{E}_{\mathrm{I}}$, and Figures 11 and 12 for $\mathcal{E}_{\mathrm{II}}$. Figures 10−12 show that the optimization of the uncertain model parameters has improved the model predictions for most of the targets. Yields are not included in the comparisons as negligible uncertainty is observed in their values and, thus, the optimization of the parameters in $\mathcal{H}$ does not affect their predictions.

To evaluate the improvement in the model predictions after the optimization, the L^2 error norm $\mathcal{E}$ is calculated between the experiments and the predictions of $\mathcal{M}_{\mathcal{P}}^{*}$ and $\mathcal{M}_{\mathcal{P}}$:

$$\mathcal{E} = \sqrt{\frac{1}{n}\sum_{i=1}^{n}\left(\frac{\eta_i(\mathbf{x}) - \eta_i^{\mathrm{obs}}}{\eta_i^{\mathrm{obs}}}\right)^2} \tag{24}$$

In eq 24, $\mathcal{E}$ for $\mathcal{M}_{\mathcal{P}}^{*}$ and $\mathcal{M}_{\mathcal{P}}$ is obtained by substituting $\mathbf{x}$ by $\mathbf{x}^*$ and $\mathbf{0}$, respectively. The values of $\mathcal{E}$ for $\mathcal{M}_{\mathcal{P}}^{*}$ and $\mathcal{M}_{\mathcal{P}}$ are found to be 0.29 and 0.34, respectively, showing that the optimization of the parameters in $\mathcal{H}$ does not provide a significant improvement (15% reduction in $\mathcal{E}$) in the model predictions even though the experimental measurements of several targets fall within the uncertainty bounds of the model predictions. This can be explained by realizing that each target can have a unique set of model parameters that minimizes the differences between the experimental measurements and the model predictions. For biomass pyrolysis, no single target can accurately characterize the overall pyrolysis process, and therefore biomass pyrolysis model must be able to predict

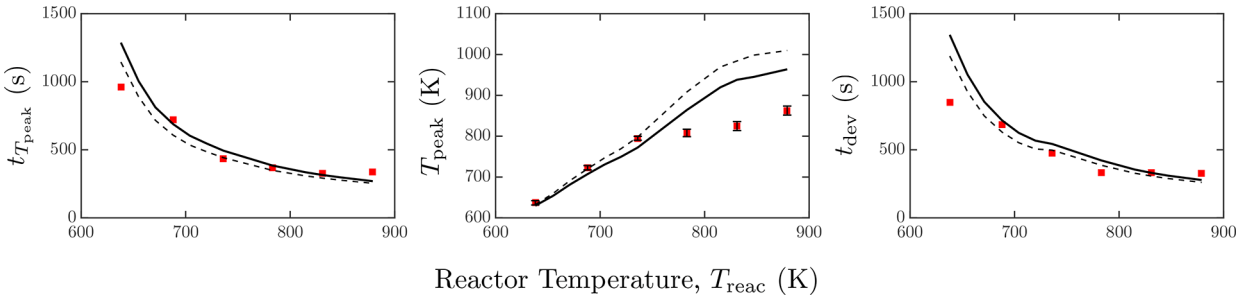

Figure 10. Comparison between the predictions of the optimized model (solid lines), the base model (dashed lines), and the experimental measurements (symbols) for the targets of $\mathcal{E}_{\mathrm{I}}$.

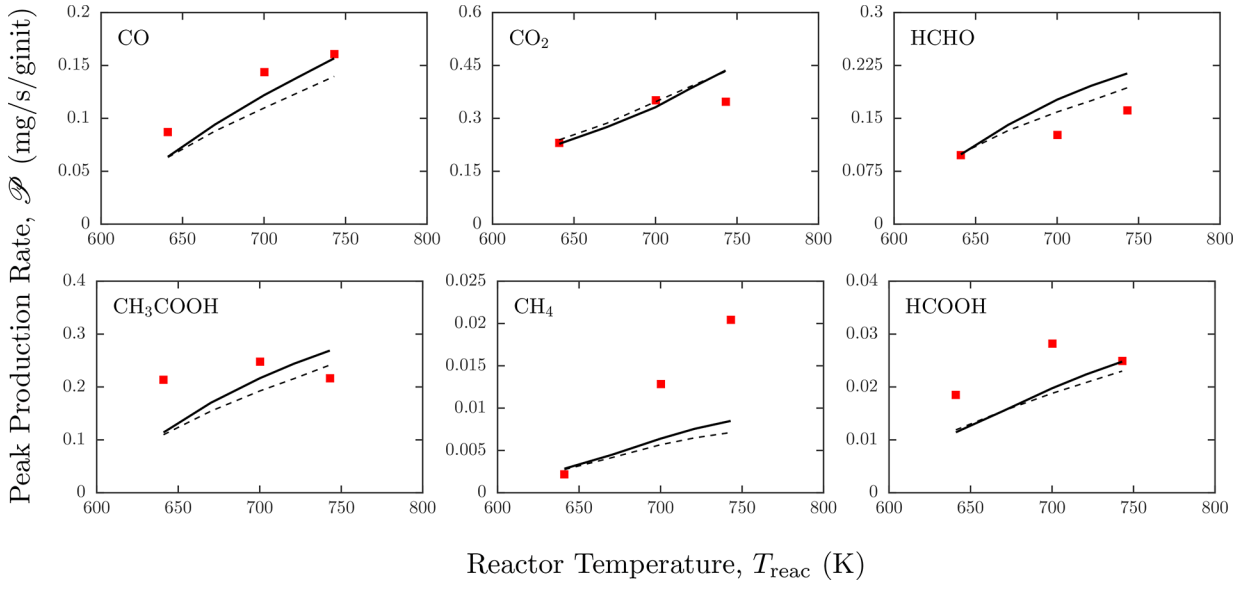

Figure 11. Maximum production rates of species $\mathcal{P}$ for $\mathcal{E}_{\mathrm{II}}$. Comparison between the predictions of the optimized model (solid lines), the base model (dashed lines), and the experimental measurements (symbols).

DOI: 10.1021/acssuschemeng.8b02493
ACS Sustainable Chem. Eng. 2018, 6, 12153−12165

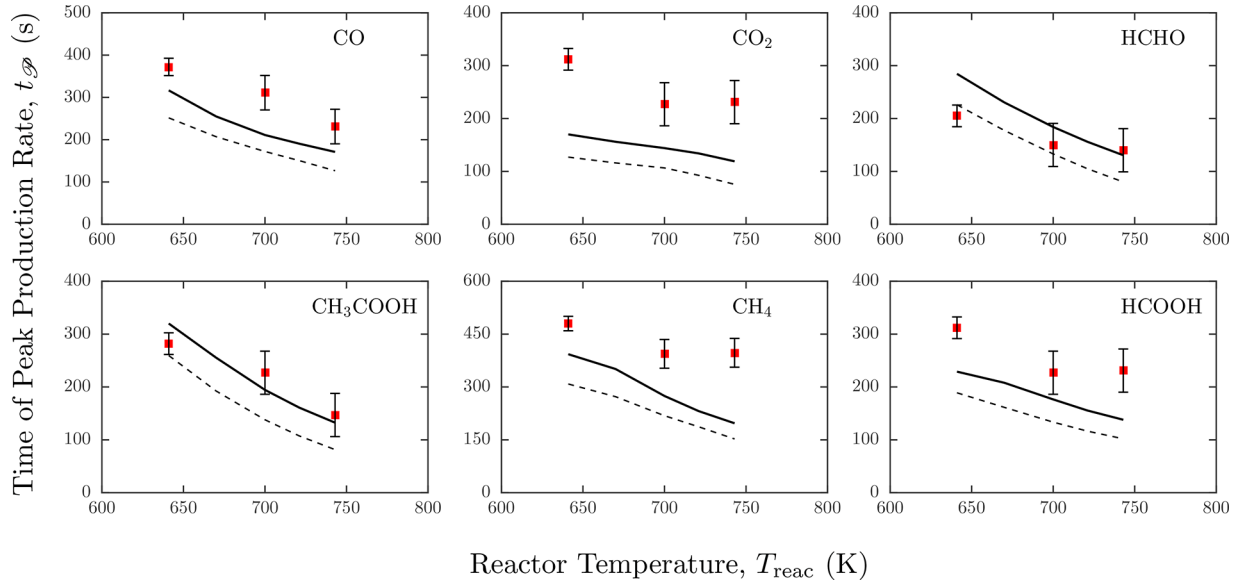

Figure 12. Time for maximum production rates of species $t_{\mathcal{P}}$ for $\mathcal{E}_{II}$. Comparison between the predictions of the optimized model (solid lines), the base model (dashed lines), and the experimental measurements (symbols).

multiple targets that are governed by different physical and chemical processes. To check how much the optimized model can be improved when only a single target is considered, we optimize the parameters in $\mathcal{H}$ for T_{peak}. We observe that the resulting optimized model provides a significant improvement in the predictions of T_{peak} as shown in Figure 13. For this case,

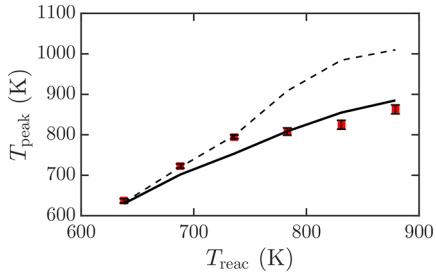

Figure 13. Comparison between the predictions of the optimized model (solid lines), the base model (dashed lines), and the experimental measurements (symbols) for the predictions of T_{peak} for $\mathcal{E}_{I}$.

75% reduction in $\mathcal{E}$ is achieved by the optimized model ($\mathcal{E}$=0.03) in comparison to the base model ($\mathcal{E}$=0.12).

The results of the optimization study have an important implication that an excellent agreement can be obtained between the model predictions and the experiments by tuning the uncertain model parameters if only a few targets are considered in the validation process. Therefore, in the presence of uncertainty in the model parameters, consideration of a wide variety of detailed experimental measurements becomes vital for a rigorous model validation.

CONCLUSIONS

In this work, a rigorous analysis of the validity of a commonly used one-dimensional particle-scale biomass pyrolysis model was performed using uncertainty quantification and the optimal values of the uncertain model parameters were evaluated. For this purpose, two detailed experimental studies of the pyrolysis of spherical wood spheres were considered from the literature. By combining sensitivity analysis and literature search, a set of sensitive transport model parameters was identified and the uncertainty in their values was characterized using uniform distribution. To perform the uncertainty propagation and the optimization of the uncertain model parameters, response surfaces were created to allow for a fast evaluation of the model predictions. The response surfaces were evaluated by sampling the PDFs of the uncertain model parameters to propagate the uncertainty through the pyrolysis model. The resulting model predictions containing the uncertainty were compared to the experimental measurements of several targets. We found that the uncertainty in the model predictions can account for most of the discrepancies related to the particle temperature profiles and the species production rates. However, the discrepancies related to the product yields and the timings of the peak production rates of a few species cannot be explained by the uncertainty. The results also showed that the pyrolysis model performs poorly in predicting all the targets related to CH_4. The experimental targets identified in this work, whose predictions cannot be improved by an accurate knowledge of the transport model parameters, can be a focus area for further developments in the chemical kinetic model.

The optimization study showed that the optimal values of the uncertain model parameters could achieve a minor improvement (15% reduction in the L^2 error norm) in the model predictions when all the targets were considered, whereas a significant improvement (75% reduction in the L^2 error norm) was obtained when only a single target (T_{peak}) was considered. This observation emphasizes the importance of considering a wide variety of experimental targets during the model validation process, as good agreement can be obtained between the model predictions and the experiments by tuning the model parameters if only a few targets are considered.

The present work is a first step toward developing the UQ methodology in the context of biomass pyrolysis, and we have made several simplifying assumptions, including the 1D spherically symmetric and isotropic representation of the biomass particle. The methodology used in this work is systematic

DOI: 10.1021/acssuschemeng.8b02493
ACS Sustainable Chem. Eng. 2018, 6, 12153−12165

and general, and provided that adequate computational resources are available, can in theory be applied to more complex simulation configurations associated with realistic biomass feedstock.

■ ASSOCIATED CONTENT

Supporting Information

The Supporting Information is available free of charge on the ACS Publications website at DOI: 10.1021/acssuschemeng.8b02493.

Input parameters used for the biomass pyrolysis simulations (PDF)

■ AUTHOR INFORMATION

Corresponding Author

*H. Goyal. E-mail: hg345@cornell.edu.

ORCID

Himanshu Goyal: 0000-0001-5387-632X

Notes

The authors declare no competing financial interest.

■ ACKNOWLEDGMENTS

This material is based in part upon work supported by the National Science Foundation under Grant CBET 1638837. The authors thank Prof. Elizabeth Fisher for her insights and useful discussions about the wood pyrolysis experiments described in Bennadji et al.[29]

■ REFERENCES

(1) Shafizadeh, F.; Chin, P. P. *Thermal deterioration of wood*; ACS Publications, 1977.

(2) Vinu, R.; Broadbelt, L. J. A mechanistic model of fast pyrolysis of glucose-based carbohydrates to predict bio-oil composition. *Energy Environ. Sci.* **2012**, *5*, 9808−9826.

(3) Zhou, X.; Nolte, M. W.; Mayes, H. B.; Shanks, B. H.; Broadbelt, L. J. Experimental and mechanistic modeling of fast pyrolysis of neat glucose-based carbohydrates. 1. Experiments and development of a detailed mechanistic model. *Ind. Eng. Chem. Res.* **2014**, *53*, 13274−13289.

(4) Gómez-Barea, A.; Leckner, B. Modeling of biomass gasification in fluidized bed. *Prog. Energy Combust. Sci.* **2010**, *36*, 444−509.

(5) Kumar, R. R.; Kolar, A. K.; Leckner, B. Shrinkage characteristics of Casuarina wood during devolatilization in a fluidized bed combustor. *Biomass Bioenergy* **2006**, *30*, 153−165.

(6) Ciesielski, P. N.; Crowley, M. F.; Nimlos, M. R.; Sanders, A. W.; Wiggins, G. M.; Robichaud, D.; Donohoe, B. S.; Foust, T. D. Biomass particle models with realistic morphology and resolved microstructure for simulations of intraparticle transport phenomena. *Energy Fuels* **2015**, *29*, 242−254.

(7) Pecha, M. B.; Garcia-Perez, M.; Foust, T. D.; Ciesielski, P. N. Estimation of Heat Transfer Coefficients for Biomass Particles by Direct Numerical Simulation Using Microstructured Particle Models in the Laminar Regime. *ACS Sustainable Chem. Eng.* **2017**, *5*, 1046−1053.

(8) Mettler, M. S.; Vlachos, D. G.; Dauenhauer, P. J. Top ten fundamental challenges of biomass pyrolysis for biofuels. *Energy Environ. Sci.* **2012**, *5*, 7797−7809.

(9) Xiong, Q.; Xu, F.; Pan, Y.; Yang, Y.; Gao, Z.; Shu, S.; Hong, K.; Bertrand, F.; Chaouki, J. Major trends and roadblocks in CFD-aided process intensification of biomass pyrolysis. *Chem. Eng. Process.* **2018**, *127*, 206.

(10) Wiggins, G. M.; Ciesielski, P. N.; Daw, C. S. Low-order modeling of internal heat transfer in biomass particle pyrolysis. *Energy Fuels* **2016**, *30*, 4960−4969.

(11) Corbetta, M.; Frassoldati, A.; Bennadji, H.; Smith, K.; Serapiglia, M. J.; Gauthier, G.; Melkior, T.; Ranzi, E.; Fisher, E. M. Pyrolysis of centimeter-scale woody biomass particles: kinetic modeling and experimental validation. *Energy Fuels* **2014**, *28*, 3884−3898.

(12) Eitelberger, J.; Hofstetter, K. Prediction of transport properties of wood below the fiber saturation point-A multiscale homogenization approach and its experimental validation: Part I: Thermal conductivity. *Compos. Sci. Technol.* **2011**, *71*, 134−144.

(13) Najm, H. N. Uncertainty quantification and polynomial chaos techniques in computational fluid dynamics. *Annu. Rev. Fluid Mech.* **2009**, *41*, 35−52.

(14) Mueller, M. E.; Pitsch, H. Large eddy simulation subfilter modeling of soot-turbulence interactions. *Phys. Fluids* **2011**, *23*, 115104.

(15) Gel, A.; Garg, R.; Tong, C.; Shahnam, M.; Guenther, C. Applying uncertainty quantification to multiphase flow computational fluid dynamics. *Powder Technol.* **2013**, *242*, 27−39.

(16) Sahraei, M. H.; Duchesne, M. A.; Hughes, R. W.; Ricardez-Sandoval, L. A. Experimental Assessment, Model Validation, and Uncertainty Quantification of a Pilot-Scale Gasifier. *Ind. Eng. Chem. Res.* **2016**, *55*, 6961−6970.

(17) Gentile, G.; Debiagi, P. E. A.; Cuoci, A.; Frassoldati, A.; Ranzi, E.; Faravelli, T. A computational framework for the pyrolysis of anisotropic biomass particles. *Chem. Eng. J.* **2017**, *321*, 458−473.

(18) Park, W. C.; Atreya, A.; Baum, H. R. Experimental and theoretical investigation of heat and mass transfer processes during wood pyrolysis. *Combust. Flame* **2010**, *157*, 481−494.

(19) Anca-Couce, A. Reaction mechanisms and multi-scale modelling of lignocellulosic biomass pyrolysis. *Prog. Energy Combust. Sci.* **2016**, *53*, 41−79.

(20) Anca-Couce, A.; Scharler, R. Modelling heat of reaction in biomass pyrolysis with detailed reaction schemes. *Fuel* **2017**, *206*, 572−579.

(21) Wang, H.; Sheen, D. A. Combustion kinetic model uncertainty quantification, propagation and minimization. *Prog. Energy Combust. Sci.* **2015**, *47*, 1−31.

(22) Frenklach, M. Systematic optimization of a detailed kinetic model using a methane ignition example. *Combust. Flame* **1984**, *58*, 69−72.

(23) Papadikis, K.; Gu, S.; Bridgwater, A. V. CFD modelling of the fast pyrolysis of biomass in fluidised bed reactors: modelling the impact of biomass shrinkage. *Chem. Eng. J.* **2009**, *149*, 417−427.

(24) Di Blasi, C. Heat, momentum and mass transport through a shrinking biomass particle exposed to thermal radiation. *Chem. Eng. Sci.* **1996**, *51*, 1121−1132.

(25) Mathur, S.; Tondon, P.; Saxena, S. Thermal conductivity of binary, ternary and quaternary mixtures of rare gases. *Mol. Phys.* **1967**, *12*, 569−579.

(26) Frenklach, M.; Wang, H.; Rabinowitz, M. J. Optimization and analysis of large chemical kinetic mechanisms using the solution mapping method-combustion of methane. *Prog. Energy Combust. Sci.* **1992**, *18*, 47−73.

(27) Box, G. E. *Statistics for experiments: An introduction to design, data analysis, and model building*; John Wiley & Sons, 1978.

(28) *COMSOL Multiphysics, User's guide*, version 4; COMSOL Inc., 2007.

(29) Bennadji, H.; Smith, K.; Serapiglia, M. J.; Fisher, E. M. Effect of particle size on low-temperature pyrolysis of woody biomass. *Energy Fuels* **2014**, *28*, 7527−7537.

(30) Bergman, T. L.; Incropera, F. P.; DeWitt, D. P.; Lavine, A. S. *Fundamentals of heat and mass transfer*; John Wiley & Sons, 2011.

(31) Di Blasi, C. Influences of physical properties on biomass devolatilization characteristics. *Fuel* **1997**, *76*, 957−964.

(32) Smith, K. A numerical study of the slow pyrolysis of thermally thick wood spheres. Ph.D. thesis, Cornell University, 2013.

(33) Gupta, M.; Yang, J.; Roy, C. Specific heat and thermal conductivity of softwood bark and softwood char particles. *Fuel* **2003**, *82*, 919−927.

(34) Hankalin, V.; Ahonen, T.; Raiko, R. On thermal properties of a pyrolysing wood particle. *Finnish-Swedish Flame Days* **2009**, *16*.

(35) Lu, H.; Ip, E.; Scott, J.; Foster, P.; Vickers, M.; Baxter, L. L. Effects of particle shape and size on devolatilization of biomass particle. *Fuel* **2010**, *89*, 1156−1168.
(36) Glass, S. V.; Zelinka, S. L. Moisture relations and physical properties of wood. *Wood handbook: wood as an engineering material: Centennial ed.*; General technical report FPL; GTR-190; U.S. Department of Agriculture, Forest Service, Forest Products Laboratory: Madison, WI, 2010; Chapter 4, pp 4.1−4.19.
(37) Sheen, D. A.; Wang, H. The method of uncertainty quantification and minimization using polynomial chaos expansions. *Combust. Flame* **2011**, *158*, 2358−2374.
(38) Curtis, L. J.; Miller, D. J. Transport model with radiative heat transfer for rapid cellulose pyrolysis. *Ind. Eng. Chem. Res.* **1988**, *27*, 1775−1783.
(39) Miller, R.; Bellan, J. A generalized biomass pyrolysis model based on superimposed cellulose, hemicelluloseand liqnin kinetics. *Combust. Sci. Technol.* **1997**, *126*, 97−137.
(40) Lathouwers, D.; Bellan, J. Yield optimization and scaling of fluidized beds for tar production from biomass. *Energy Fuels* **2001**, *15*, 1247−1262.
(41) Xiong, Q.; Kong, S.-C. High-resolution particle-scale simulation of biomass pyrolysis. *ACS Sustainable Chem. Eng.* **2016**, *4*, 5456−5461.
(42) Blondeau, J.; Jeanmart, H. Biomass pyrolysis at high temperatures: Prediction of gaseous species yields from an anisotropic particle. *Biomass Bioenergy* **2012**, *41*, 107−121.
(43) Koch, P. Specific heat of ovendry spruce pine wood and bark. *Wood Sci.* **1968**, *1* (4), 203−214.
(44) Harada, T.; Hata, T.; Ishihara, S. Thermal constants of wood during the heating process measured with the laser flash method. *J. Wood Sci.* **1998**, *44*, 425−431.
(45) Gronli, M. A theoretical and experimental study of the thermal degradation of biomass. Ph.D. thesis, The Norwegian University on Science and Technology, 1996.
(46) Ragland, K.; Aerts, D.; Baker, A. Properties of wood for combustion analysis. *Bioresour. Technol.* **1991**, *37*, 161−168.
(47) Simpson, W.; TenWolde, A. *The Encyclopedia of Wood*; Skyhorse Publishing, 1999.
(48) Koufopanos, C.; Maschio, G.; Lucchesi, A. Pyrolysis kinetics of wood and wood components. *Can. J. Chem. Eng.* **1989**, *7*, 67−75.
(49) Babu, B.; Chaurasia, A. Pyrolysis of biomass: improved models for simultaneous kinetics and transport of heat, mass and momentum. *Energy Convers. Manage.* **2004**, *45*, 1297−1327.
(50) Stull, D. R.; Prophet, H. *JANAF thermochemical tables*; U.S. National Bureau of Standards, 1971.
(51) Fredlund, B. A model for heat and mass transfer in timber structures during fire: a theoretical, numerical and experimental study. Ph.D. thesis, Lund University, Department of Fire Safety Engineering, 1988.
(52) Larfeldt, J.; Leckner, B.; Melaaen, M. C. Modelling and measurements of heat transfer in charcoal from pyrolysis of large wood particles. *Biomass Bioenergy* **2000**, *18*, 507−514.
(53) Pyle, D.; Zaror, C. Heat transfer and kinetics in the low temperature pyrolysis of solids. *Chem. Eng. Sci.* **1984**, *39*, 147−158.
(54) Lee, C. K.; Chaiken, R. F.; Singer, J. M. Charring pyrolysis of wood in fires by laser simulation. *Symposium (International) on Combustion*, 1977; pp 1459−1470.
(55) Thunman, H.; Leckner, B. Thermal conductivity of wood models for different stages of combustion. *Biomass Bioenergy* **2002**, *23*, 47−54.
(56) Leon, G.; Cruz-de Leon, J.; Villasenor, L. Thermal characterization of pine wood by photoacoustic and photothermal techniques. *Holz als Roh-und Werkstoff* **2000**, *58*, 241−246.
(57) Suleiman, B.; Larfeldt, J.; Leckner, B.; Gustavsson, M. Thermal conductivity and diffusivity of wood. *Wood Sci. Technol.* **1999**, *33*, 465−473.
(58) Anca-Couce, A.; Sommersacher, P.; Scharler, R. Online experiments and modelling with a detailed reaction scheme of single particle biomass pyrolysis. *J. Anal. Appl. Pyrolysis* **2017**, *127*, 411−425.
(59) Goyal, H.; Pepiot, P. A compact kinetic model for biomass pyrolysis at gasification conditions. *Energy Fuels* **2017**, *31*, 12120−12132.
(60) Brook, A.; Kendrick, D.; Meeraus, A. GAMS, a user's guide. *ACM Signum Newsletter* **1988**, *23*, 10−11.

DOI: 10.1021/acssuschemeng.8b02493
ACS Sustainable Chem. Eng. 2018, 6, 12153−12165